Time-delayed coincidence technique for subnatural-width spectroscopy as an interference phenomenon

R. N. Shakhmuratov[1,2] and F. G. Vagizov[2]

[1]*Kazan Physical-Technical Institute, FRC Kazan Scientific Center of RAS, 10/7 Sibirsky Trakt, Kazan 420029, Russia*

[2]*Kazan Federal University, 18 Kremlyovskaya Street, Kazan 420008, Russia*

(Received 21 December 2018; published 18 March 2019)

A single photon, emitted in a transition between two states, has a frequency distribution of intensity that is given by a Lorentzian if the transition is only naturally broadened and the period of observation T is long compared to the lifetime T_1 of the excited state. However, when the observation time T is short or comparable to T_1, the frequency spectrum is appreciably broadened. If only the delayed part of the emitted radiation field is detected, then the radiation spectrum does not change. However, if the radiation field is transmitted through a resonant absorber and then detected, the transmission spectrum of the delayed radiation field is narrowed. We show that this narrowing is due to the interference of the spectral components of the incident and coherently scattered fields. Experimental spectra of absorption of Mössbauer radiation, obtained by the coincidence technique, confirm this conclusion.

DOI: 10.1103/PhysRevA.99.033831

I. INTRODUCTION

The intensity distribution of a line emitted in a transition between two quantum states is given by a Lorentzian if the line is only naturally broadened and the period of observation T is long. However, when time T is short or comparable to the lifetime T_1 of the excited state, the frequency spectrum of the emitted radiation is appreciably broadened. Experiments with gamma photons clearly demonstrated the spectrum broadening when $T < T_1$ [1–4]. These experiments make use of the coincidence-Mössbauer technique, which could be summarized for ^{57}Fe as follows. The source nucleus, ^{57}Co, undergoes electron capture to form a second excited state of ^{57}Fe whose lifetime is 12 ns. This state decays via two-photon cascade emitting sequentially 122- and 14.4-keV photons. Detection of the 122-keV photon signals the occupation of the 14.4-keV excited state of ^{57}Fe whose lifetime is 141 ns. This allows one to use the Mössbauer spectroscopy selecting only those 14.4-keV photons that are emitted during some preset time interval after detecting the 122-keV photon. Such a "time filtering" results in substantial modification of the experimentally observed transmission-line shape.

The coincidence-Mössbauer spectroscopy was applied in [3–5] to improve the spectral resolution by taking spectra counting only those gamma photons coming from the source nucleus that have lived longer than one lifetime. Appreciable line narrowing was explained by the argument that photons, emitted by nuclei that have lived a longer time, have a better defined energy [6]. A similar technique was also applied in an optical domain, and it was called time-biased coherent spectroscopy since it is based on selectively discarding that part of the signal arriving shortly after the excitation of the state to be studied (for a review, see [7]). Significant linewidth reduction in this technique has resulted in substantial improvements in precision. The gain is attained when one observes the radiation from naturally decaying states a certain time interval after they are populated and, therefore, limits data collection to the set of atoms that have survived in the excited state for a longer time than average. In the optical domain, the time-biased technique was successfully applied in double resonance [8] and level-crossing [9,10] experiments.

In this paper, we show that spectral resolution in time-biased coherent spectroscopy originates from the interference phenomena. While in the optical domain this is an obvious conclusion since the line narrowing effects occur only when the phase of the decaying signal is preserved by a measuring process (see, for example, [11]), in the gamma domain the line narrowing is usually explained by a decrease of the energy uncertainty of photons emitted at a later time [3–5]. We show theoretically that the spectrum of photons, detected with an appreciable delay after the excited state population of the source nucleus, does not experience narrowing. The experimentally observed narrowing of the transmission line of the radiation field, detected with a large delay, is due to the interference of the spectral components of the incident and coherently scattered fields. We also derive a simple formula for estimation of the spectral resolution in the gamma domain.

II. SPECTRUM OF AN EMITTED PHOTON IN TIME-BIASED MEASUREMENTS

Lynch *et al.* [12] empirically introduced an expression for the source photon within a classical theory of gamma photon propagation in a dense resonant absorber. A single-photon radiation field is presented as a damping electric field

$$a(t) = \Theta(t)e^{-i\omega_S t-\Gamma_S t/2}, \tag{1}$$

where the distance from the source is neglected, the amplitude of the field at the input of the absorber is normalized to unity, time t_0 when the source nucleus is formed in the excited state is defined as $t_0 = 0$, $\Theta(t)$ is the Heaviside step function, ω_S is the frequency of the resonant transition from the excited to

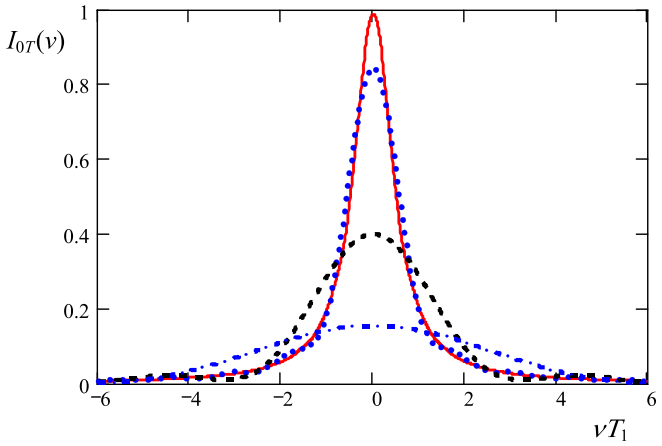

FIG. 1. Power spectrum of the source radiation field, seen by the frequency selective detector in a thought experiment. The opening time T of the shutter is $10T_1$ (solid red line), $5T_1$ (dotted blue line), $2T_1$ (dashed black line), and T_1 (dash-dotted blue line).

the ground state, and Γ_S is the reciprocal of the mean lifetime of the excited state T_1, i.e., $\Gamma_S = 1/T_1$.

If we adopt the Fourier transform of the form

$$F(\omega) = \int_{-\infty}^{+\infty} f(t)e^{i\omega t}dt, \tag{2}$$

the Fourier transform of the radiation field amplitude (1) is

$$A(\omega) = \frac{1}{\Gamma_S/2 - i(\omega - \omega_S)}, \tag{3}$$

and its intensity distribution $I(\omega) = A(\omega)A^*(\omega)$ is given by the Lorentzian function

$$I(\omega) = \frac{1}{(\Gamma_S/2)^2 + (\omega - \omega_S)^2}. \tag{4}$$

Assume a shutter is available in the gamma domain, and we place this shutter between the source and the detector. In this gedanken experiment, we also suppose that our detector is capable of measuring the spectral content of the radiation field. Below we consider two cases, i.e., (i) the shutter is open in a time interval $(0, T)$ allowing detection only of a leading edge of a single-photon wave packet, and (ii) the shutter is open $(T, +\infty)$ to detect only the tail of a single-photon wave packet.

In the first case, the probability amplitude of the photon, transmitted by the shutter, is

$$a_{0T}(t) = a(t)[1 - \Theta(t - T)], \tag{5}$$

and its Fourier transform

$$A_{0T}(\omega) = \frac{1 - e^{i(\omega-\omega_S)T-\Gamma_S T/2}}{\Gamma/2 - i(\omega - \omega_S)} \tag{6}$$

gives the following expression for the radiation intensity [1]:

$$I_{0T}(\nu) = \frac{1 + e^{-\Gamma_S T} - 2e^{-\Gamma_S T/2}\cos\nu T}{(\Gamma_S/2)^2 + \nu^2}, \tag{7}$$

where $\nu = \omega - \omega_S$. For a long-time interval when the shutter is open, the radiation spectrum is close to Lorentzian (4); see Fig. 1, the solid red line, which corresponds to $T = 10T_1$. With time-interval shortening, the spectrum broadens. For example, for $T = T_1$ the spectrum width increases 5.6 times (see Fig. 1, dash-dotted blue line). The drop of intensity at the line center $\nu = 0$ is due to discarding an appreciable part of a single-photon pulse, and it is described by the equation

$$I_{0T}(0) = \frac{(1 - e^{-\Gamma_S T/2})^2}{(\Gamma/2)^2}. \tag{8}$$

For T close to T_1, the intensity drops slightly more than two times with respect to the line center when $\nu T = \pm\pi$. For these frequencies, Eq. (7) is simplified as follows:

$$I_{0T}(\pm\pi/T) = \frac{(1 + e^{-\Gamma_S T/2})^2}{(\Gamma_S/2)^2 + (\pi/T)^2}. \tag{9}$$

Thus, when $T = T_1$, the half-width at half-maximum of the radiation field increases almost 2π times.

This result also follows from simple properties of the Fourier transforms. Since the probability amplitude of the truncated photon, Eq. (5), is a product of $a(t)$, Eq. (1), and a rectangular function $f_R(t) = \Theta(t)[1 - \Theta(t - T)]$, the Fourier transform of Eq. (5) is a convolution of the Fourier transforms of the probability amplitude of the nontruncated photon $A(\omega)$ and the rectangular function $F_R(\omega)$, i.e.,

$$A_{0T}(\nu) = \frac{1}{2\pi}\int_{-\infty}^{+\infty} A(\nu_1)F_R(\nu - \nu_1)d\nu_1, \tag{10}$$

where $\nu = \omega - \omega_0$ and

$$F_R(\nu) = Te^{i\nu T/2}\frac{\sin\nu T/2}{\nu T/2}. \tag{11}$$

For $T \ll T_1$, the half-width at half-maximum of $F_R(\nu)$ is π/T, which is much larger than that of $A(\nu_1)$. Therefore, the width of $F_R(\nu)$ defines the width of the truncated photon $A_{0T}(\nu)$ for short observation time T.

If the shutter is open at time T for a long-time interval $(T, +\infty)$, the probability amplitude of the photon transmitted by the shutter is

$$a_{T\infty}(t) = \Theta(t - T)a(t). \tag{12}$$

Its Fourier transform

$$A_{T\infty}(\nu) = \frac{e^{i\nu T-\Gamma_S T/2}}{\Gamma_S/2 - i\nu} \tag{13}$$

gives the following expression for the radiation intensity:

$$I_{T\infty}(\nu) = \frac{e^{-\Gamma T}}{(\Gamma_S/2)^2 + \nu^2}, \tag{14}$$

which differs from the Lorentzian profile (4) only by the numerical factor $\exp(-T)$. Thus, there is no spectrum narrowing of photons, which are detected at a later time.

In the gamma domain, the shutters and spectrum selective detectors are not yet available. Instead, the time-delayed coincidence counting technique and resonant absorbers are used [1–5]. While transmission spectrum broadening detected by this technique [1–4] confirms the spectrum broadening of a photon for the observation time interval $(0, T)$, the line narrowing in the time interval $(T, +\infty)$ could be explained

only by the interference phenomenon since the photon spectrum is not narrowed in delayed detection. This point will be discussed in the next section.

III. COINCIDENCE-MÖSSBAUER SPECTROSCOPY

Lynch *et al.* [12] proposed describing the time dependence of the radiation field amplitude of the source, Eq. (1), which is transmitted through the absorber of physical thickness L, by an inverse Fourier transformation,

$$a_{\rm out}(t-t_0)=\frac{1}{2\pi}\int_{-\infty}^{+\infty}A_{\rm out}(\omega)e^{-i\omega(t-t_0)}d\omega, \tag{15}$$

where $A_{\rm out}(\omega)=A(\omega)\exp[-\alpha_A(\omega)L/2]$ is the radiation spectrum at the exit of the absorber, $A(\omega)$ is the spectrum of the incident radiation field [see Eq. (3)], t_0 is the time when the excited state nucleus is formed in the source, $\alpha(\omega)$ is the complex dielectric constant, which describes frequency-dependent absorption and the phase shift of the field in the sample, and L is the absorber physical thickness. For the absorber with a single resonance line, $\alpha_A(\omega)$ is

$$\alpha_A(\omega)=\frac{i\Gamma_A d/2L}{\omega-\omega_A+i\Gamma_A/2}, \tag{16}$$

where ω_A and Γ_A are the resonant frequency and absorption linewidth of nuclei, $d=n_A\sigma f_A L$ is the optical thickness of the absorber, n_A is the number of nuclei per unit volume of the absorber, σ is the resonance absorption cross section, and f_A is the recoilless fraction of gamma ray absorption. If we count a number of photons, detected within long time intervals of the same duration for different values of the detuning from resonance, $\Delta=\omega_S-\omega_A$, we obtain the Mössbauer spectrum showing the dependence of transmitted radiation intensity on Δ. This number of counts is

$$n_\infty(\Delta)=\int_{-\infty}^{+\infty}n_{\rm out}(t-t_0)dt, \tag{17}$$

where $n_{\rm out}(t-t_0)=|a_{\rm out}(t-t_0)|^2$. If we express $n_{\rm out}(t-t_0)$ as

$$n_{\rm out}(t-t_0)=\frac{1}{(2\pi)^2}\int_{-\infty}^{+\infty}d\omega_1\int_{-\infty}^{+\infty}d\omega_2 A_{\rm out}(\omega_1)A^*_{\rm out}(\omega_2)e^{i(\omega_2-\omega_1)(t-t_0)}, \tag{18}$$

then, from Eq. (17) and the definition of the Dirac delta function,

$$\frac{1}{2\pi}\int_{-\infty}^{+\infty}e^{i(\omega_2-\omega_1)(t-t_0)}dt_0=\delta(\omega_1-\omega_2), \tag{19}$$

we obtain

$$n_\infty(\Delta)=\frac{1}{2\pi}\int_{-\infty}^{+\infty}d\omega A_{\rm out}(\omega)A^*_{\rm out}(\omega), \tag{20}$$

which is a well-known expression for transmitted radiation in Mössbauer spectroscopy [13]. Here, nonresonant absorption is disregarded. Recoil processes in nuclear emission are not taken into account assuming that the recoilless fraction of the source emission (Debye-Waller factor) is $f_S=1$. These processes can be easily taken into account in experimental data analysis.

A. Photon counts in a short time interval starting immediately after the formation of the excited state nucleus in the source

In the time-delayed coincidence technique, we are able to collect photon counts, which are detected in a time interval (t_0, t_0+T). These counts satisfy the equation

$$n_{0T}(\Delta)=\int_{t_0}^{t_0+T}n_{\rm out}(t-t_0)dt. \tag{21}$$

Substituting an integral representation of $a_{\rm out}(t-t_0)$ and $a^*_{\rm out}(t-t_0)$ via Fourier transforms $A_{\rm out}(\omega)$ and $A^*_{\rm out}(\omega)$, Eq. (15), into $n_{\rm out}(t-t_0)=a_{\rm out}(t-t_0)a^*_{\rm out}(t-t_0)$ and taking into account the relation

$$\int_{t_0}^{t_0+T}e^{i(\omega_2-\omega_1)(t-t_0)}dt=Te^{i(\omega_2-\omega_1)T/2}\frac{\sin[(\omega_2-\omega_1)T/2]}{(\omega_2-\omega_1)T/2}, \tag{22}$$

we obtain

$$n_{0T}(\Delta)=\frac{1}{(2\pi)^2}\int_{-\infty}^{+\infty}d\omega_1\int_{-\infty}^{+\infty}d\omega_2 A_{\rm out}(\omega_1)A^*_{\rm out}(\omega_2)F_R(\omega_2-\omega_1), \tag{23}$$

where $F_R(\omega_2-\omega_1)$ is the function that is defined in Eq. (11) and coincides with that on the right-hand side of Eq. (22). Thus, in the time-delayed coincidence technique we measure the interference of spectral components $A_{\rm out}(\omega_1)$ and $A^*_{\rm out}(\omega_2)$, which is governed by the spectral function $F_R(\omega_2-\omega_1)$ whose width is defined by duration T of the observation time window.

Equation (20) is consistent with Parseval's theorem, which is written as

$$\int_{-\infty}^{+\infty}a_{\rm out}(t-t_0)a^*_{\rm out}(t-t_0)dt=\frac{1}{2\pi}\int_{-\infty}^{+\infty}A_{\rm out}(\omega)A^*_{\rm out}(\omega)d\omega. \tag{24}$$

However, if we limit the time integration interval to $(0, T)$, then the relation between $a_{\rm out}(t-t_0)a^*_{\rm out}(t-t_0)$ and $A_{\rm out}(\omega)A^*_{\rm out}(\omega)$ changes to Eq. (23), where we have interference of spectral components $A_{\rm out}(\omega_1)$ and $A^*_{\rm out}(\omega_2)$ governed by the spectral function $F_R(\omega_2-\omega_1)$.

This change can be explained by the spectral broadening of the radiation field at the exit of the absorber if we shorten the observation time interval. According to Eq. (10), the spectrum broadening is described by the equation

$$\mathcal{A}_{0T}(\nu)=\frac{1}{2\pi}\int_{-\infty}^{+\infty}A_{\rm out}(\nu_1)F_R(\nu-\nu_1)d\nu_1. \tag{25}$$

For the spectrum of the radiation field at the exit of the absorber, which is calculated in a time interval $(0, T)$, Parseval's theorem holds, i.e.,

$$n_{0T}(\Delta)=\frac{1}{2\pi}\int_{-\infty}^{+\infty}d\omega\,\mathcal{A}_{0T}(\omega)\mathcal{A}^*_{0T}(\omega). \tag{26}$$

To facilitate numerical calculation of the integrals in Eq. (23), we present them with the help of substitution $\omega_\pm = \omega_2 \pm \omega_1$ as

$$n_{0T}(\Delta) = \frac{1}{2(2\pi)^2}\int_{-\infty}^{+\infty} d\omega_+ \int_{-\infty}^{+\infty} d\omega_- A_{\text{out}}\left(\frac{\omega_+ - \omega_-}{2}\right) \times A^*_{\text{out}}\left(\frac{\omega_+ + \omega_-}{2}\right) F_R(\omega_-). \quad (27)$$

It is possible to verify the accuracy of this expression if we calculate numerically the integral in Eq. (21) for $n_{0T}(\Delta)$. Analytical expression for the amplitudes $a_{\text{out}}(t-t_0)$ and $a^*_{\text{out}}(t-t_0)$ in this integral can be found in Ref. [12], where they were calculated for $\Gamma_A = \Gamma_S$. For practical use when $\Gamma_A \neq \Gamma_S$, the condition that is often met in experiment, we also calculated analytically $a_{\text{out}}(t-t_0)$ for $\Gamma_A \neq \Gamma_S$. The result is

$$a_{\text{out}}(t) = \Theta(t) e^{-(\Gamma_A/2 + i\omega_A)t} \sum_{n=0}^{+\infty} \left[s\left(\frac{t}{b}\right)^{1/2} \right]^n J_n(2\sqrt{bt}), \quad (28)$$

or

$$a_{\text{out}}(t) = \Theta(t) e^{-(\Gamma_S/2 + i\omega_S)t} \times \left[e^{-b/s} - e^{-st} \sum_{n=1}^{+\infty} (-b/s)^n \frac{J_n(2\sqrt{bt})}{(bt)^{n/2}} \right], \quad (29)$$

where $s = (\Gamma_A - \Gamma_S) - i\Delta$, $b = \Gamma_A d/4$, and $J_n(x)$ is the nth-order Bessel function; see also Ref. [14].

Moreover, it is possible to calculate the amplitude of the radiation field at the exit of the absorber with the help of the response function technique [15,16], which gives

$$a_{\text{out}}(t) = \int_{-\infty}^{+\infty} a(t-\tau) R(\tau) d\tau, \quad (30)$$

where $a(t)$ is defined in Eq. (1) and

$$R(t) = \delta(t) - e^{-(\Gamma_A + i\omega_A)t} \Theta(t) \sqrt{\frac{b}{t}} J_1(2\sqrt{bt}) \quad (31)$$

is the response function (or Green function) of a single line absorber. Equation (30) is reduced to

$$a_{\text{out}}(t) = a(t)\left[e^{-st} J_0(2\sqrt{bt}) + s\int_0^t e^{-s\tau} J_0(2\sqrt{b\tau}) d\tau \right], \quad (32)$$

which is easy to calculate numerically because the integrand is smooth and not a fast oscillating function.

The frequency dependencies of the number of counts for the infinite-time interval $n_\infty(\Delta)$, Eq. (20), and the short-time interval $n_{0T}(\Delta)$, Eq. (23), are shown in Fig. 2. The transmission spectrum measured in a short-time interval is appreciably broadened. The results of spectrum calculation by formulas (27) and (21) are coincident.

B. Analytical results for a short-time interval

To analyze analytically the spectrum broadening in coincidence-Mössbauer spectroscopy, we consider an absorber of moderate thickness d. Then, the exponential function in $A_{\text{out}}(\omega)$ can be approximated as

$$e^{-\alpha_A(\omega)L/2} = 1 - a_1 x + a_2 x^2 + \varepsilon(x), \quad (33)$$

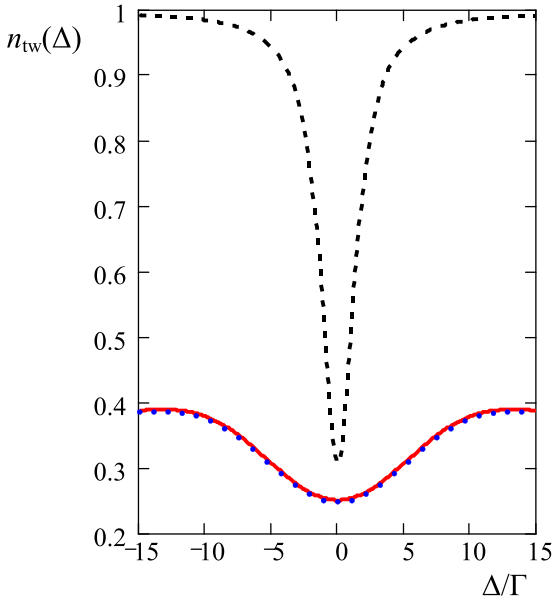

FIG. 2. Dependence of the number of counts on the detuning Δ, which are collected in different time windows $n_{\text{tw}}(\Delta)$. Here the index "tw" denotes time window. The number of counts is normalized to unity for $n_\infty(\pm\infty)$. The dashed black line shows the case when the time window is $(0, \infty)$. The solid red line and the dotted blue line show the case when the time window $(0, T)$ is short, i.e., $T = T_1/2 = 1/2\Gamma$. Spectra are plotted for $\Gamma_A = \Gamma_S = \Gamma$ and optical thickness $d = 4$. The solid red line is plotted in accord with Eq. (21), while the dotted blue line corresponds to Eq. (27).

where $x = \alpha_A(\omega)L/2$, $a_1 = 0.9664$, $a_2 = 0.3536$, and $|\varepsilon(x)| \leqslant 3 \times 10^{-3}$ if $0 \leqslant |x| \leqslant \ln 2$; see Ref. [17]. This approximation is valid if $d \leqslant 1.386$.

For simplicity, we limit our consideration to the case $\Gamma_A = \Gamma_S = \Gamma$. Then, with the help of approximation (33) we calculated analytical expressions for the infinite-time spectrum $n_\infty(\Delta)$, Eq. (20), and the spectrum $n_{0T}(\Delta)$, which is detected in a short-time interval, Eq. (23). The results are presented in the Appendix. Analysis of these expressions allowed us to derive an analytical approximation for $n_{0T}(\Delta)$, which is valid for arbitrary values of the effective thickness of the absorber d. This expression is

$$n_{0T}(\Delta) \approx \frac{1}{\Gamma}(1 - e^{-\Gamma T}) - K_{\text{B}}(d, T) L_{\text{b}}(\Delta, T), \quad (34)$$

where

$$L_{\text{b}}(\Delta, T) = \frac{\Gamma}{\Delta^2 + \Gamma^2} - e^{-\Gamma T} \frac{\sin(\Delta T + \psi)}{\Delta\sqrt{1 + \frac{\Delta^2}{\Gamma^2}}} \quad (35)$$

is the function describing the frequency dependence of photon counts $n_{0T}(\Delta)$ and $\psi = \tan^{-1}(\Delta/\Gamma)$. The numerical coefficient

$$K_{\text{B}}(d, T) = \frac{1 - e^{-\Gamma T} - \Gamma n_{0T}(0)}{1 - e^{-\Gamma T}(1 + \Gamma T)} \quad (36)$$

gives the correct value of the dip in the transmission spectrum $n_{0T}(\Delta)$. Here, the number of counts $n_{0T}(0)$ for $\Delta = 0$ is calculated numerically with the help of Eq. (21) for a given value of d, which is not small.

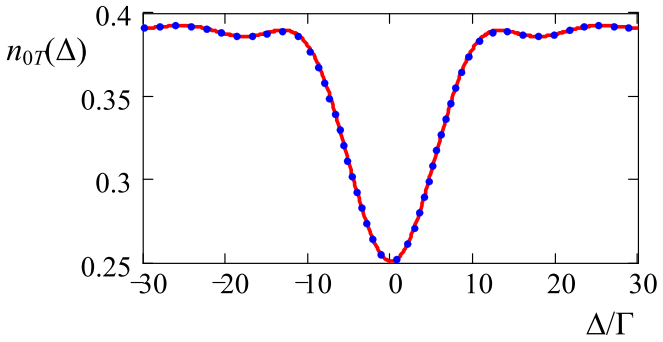

FIG. 3. Time spectrum collected in a short time interval $(0, T)$, where $T = T_1/2$. The effective thickness of the absorber is $d = 4$. The analytical approximation, Eq. (34), is shown by a red solid line, and the exact numerical calculation by a blue dotted line.

Comparison of the approximation (34) with the numerically calculated exact result for $n_{0T}(\Delta)$ is shown in Fig. 3 for $d = 4$ and $T = T_1/2$. These functions are indistinguishable.

The width of the transmission line, which is defined by the function $L_b(\Delta, T)$, originates from the competition between two terms in Eq. (35), i.e., the Lorentzian, $\Gamma/(\Delta^2 + \Gamma^2)$, and the sinc function, $\sin(\Delta T + \psi)/\Delta$. Numerical analysis shows that if $T = T_1/2$, the transmission line becomes six times broader than the Lorentzian.

C. Analytical results for delayed photon counts

Using a similar approach (see the Appendix), we derived the approximate expression for the delayed photon counts, which is

$$n_{T\infty}(\Delta) \approx \frac{e^{-\Gamma T}}{\Gamma}\left[1 - K_N(d, T)\frac{\Gamma^2 \sin(\Delta T + \psi)}{\Delta\sqrt{\Gamma^2 + \Delta^2}}\right], \quad (37)$$

where

$$K_N(d, T) = \frac{1 - \Gamma n_{T\infty}(0) e^{\Gamma T}}{1 + \Gamma T}, \quad (38)$$

and $n_{T\infty}(0) = n_\infty(0) - n_{0T}(0)$ is the number of counts in resonance ($\Delta = 0$), which is calculated numerically with the help of Eqs. (20) and (21) for a given value of d, which is not small. In the case $\Gamma_A = \Gamma_S = \Gamma$, one can use the exact expression $n_\infty(0) = \exp(-d/2) I_0(d/2)/\Gamma$, Ref. [18], for the value of the dip in the transmission spectrum measured by a traditional technique. Here, $I_0(d/2)$ is the modified Bessel function of zero order.

Analysis of Eq. (37) shows that for long delay time, $T > T_1$, the width of the transmission dip is mainly defined by the sinc function, $\sin(\Delta T + \psi)/\Delta$. For example, if $T = 2T_1 = 2/\Gamma$, the sinc function reaches its first zero at $\Delta = 1.14\Gamma$. This detuning corresponds to the first maximum of the transmission spectrum. Therefore, the half-width of the absorption dip in the spectrum is located between $\Delta = 0$ and $\Delta = 1.14\Gamma$. This half-width is equal to 0.57Γ, i.e., it becomes nearly two times smaller than the half-width of the stationary spectrum. Thus, narrowing of the time-delayed spectra is obvious.

Figure 4 shows a comparison of the numerically calculated exact function $n_{T\infty}(\Delta)$ and approximation, Eq. (37).

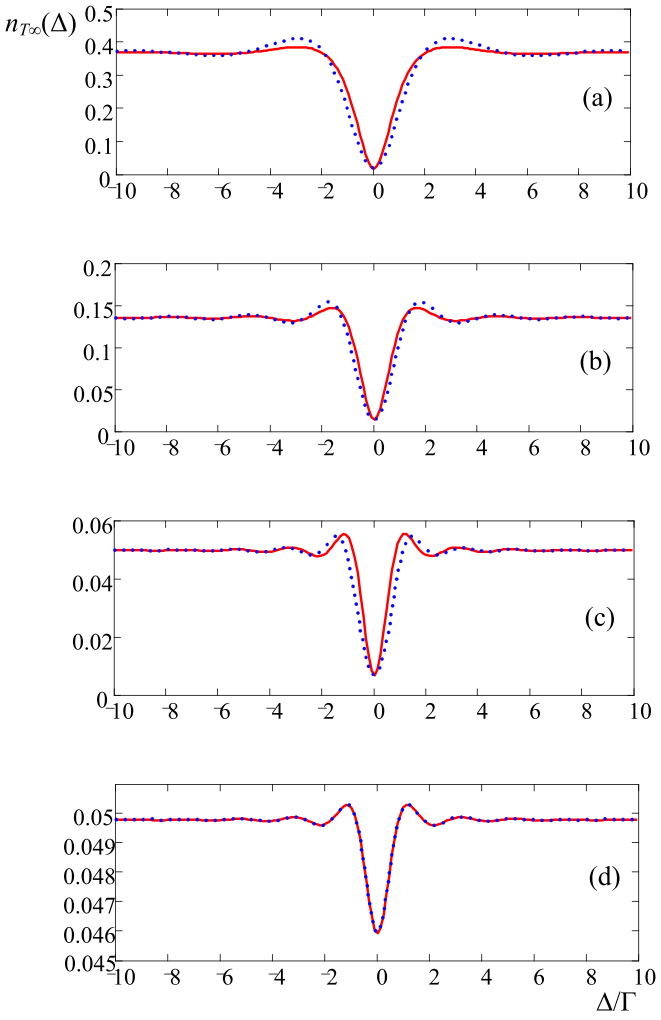

FIG. 4. Time spectrum collected in a time interval (T, ∞), where (a) $T = T_1$, (b) $T = 2T_1$, and (c) $T = 3T_1$. Effective thickness of the absorber is $d = 4$ in (a)–(c) and $d = 0.04$ in (c). The analytical approximation, Eq. (37), is shown by a red solid line, and the exact numerical calculation by a blue dotted line.

Qualitatively these functions are similar. The small difference between them originates from the thickness broadening of the transmission line.

It is interesting to notice that, for example, for the absorber with an effective thickness $d = 4$, the transmission line, collected an infinite time, broadens 1.54 times, i.e., its half-width is equal to 1.54Γ. If we collect the transmission spectrum with a delay $T = 2T_1$, then the approximate expression predicts a half-width 0.57Γ, while numerical calculation gives 0.72Γ. Thus, line narrowing by the factor 2–3 compared with the traditional technique is achieved for these parameters.

Interference of the incident and coherently scattered radiation fields plays a crucial role in the line narrowing effect. This is because the radiation field of the source and the radiation field coherently scattered by nuclei in the absorber have different frequencies, i.e., ω_S and ω_A, respectively; see Eq. (30) and the structure of the response function in Eq. (31). One can find a discussion of this point in Ref. [19]. Interference of the fields results in intensity beats with frequency $\Delta =$

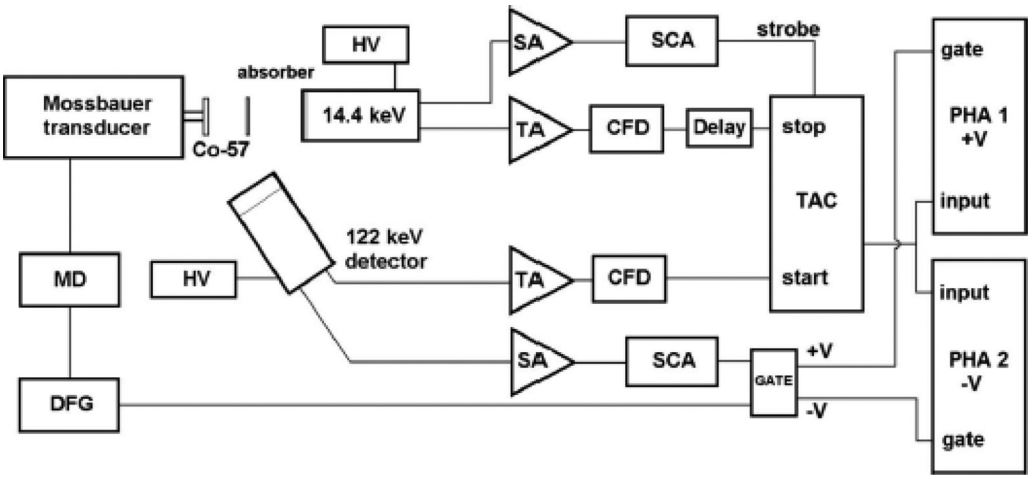

FIG. 5. Simplified scheme of the experimental setup. TAC is a time-to-amplitude converter. PHA is a pulse-height analyzer. TA is a timing amplifier. SA is a spectroscopy amplifier. SCA is a single-channel analyzer. DFG-MD is the Mössbauer driving unit and function generator. HV is a high-voltage supply.

$\omega_S - \omega_A$. If we discard photon counts within a time interval $(0, T)$ corresponding to the leading edge of a single-photon wave packet, the phase shift ΔT, accumulated in this interval between the fields, will be revealed in the signal detected at a later time. If $T > T_1$, this interference results in the line narrowing effect.

IV. EXPERIMENT

Our experimental setup is based on an ordinary delayed coincidence scheme usually used in measurements of the lifetimes of nuclear states. The schematic arrangement of the source, absorber, detectors, and electronics is shown in Fig. 5. The source ^{57}Co incorporated in the Rh matrix, with 0.14 MBq activity, is mounted on the holder of the Mössbauer drive, which is used to Doppler-shift the frequency of the radiation of the source. The absorber was made of enriched $K_4Fe(CN)_6 \cdot 3H_2O$ powder with an effective thickness $d = 13.2$. To calibrate a time resolution of our setup, we measured a time spectrum of the decay of the 14.4 keV state with no absorber. A time resolution of 9.1(5) ns was obtained by least-squares-fitting the experimental lifetime spectra with the convolution of the theoretical decay curve and a Gaussian distribution originating from the time resolution function of the experimental setup (see, for example, Ref. [19] for the procedure). The curve measured for a single line source ^{57}Co shows the single exponential decay with a mean lifetime $T_1 = 1/\Gamma$ of 140(9) ns, in good agreement with the mean lifetime and the natural linewidth data for the 14.4 keV state of ^{57}Fe.

The decay curve of the radiation field from the source along with time windows where photon counts were collected to plot delayed spectra are shown in Fig. 6. The background due to accidental coincidences is subtracted from the data. This background is defined from the counting rate at times preceding the fast front of the incident radiation pulses.

Transmission spectra obtained for different time windows are shown in Fig. 7. When the time window is short, i.e., for $\delta_1 = 38$ ns with $t_1 = 2$ ns and $t_2 = 40$ ns, the line is appreciably broadened [see Fig. 7(a)]. Then, with increasing t_1 and lengthening time interval δ_n, the line narrows. The narrowest line is obtained for $\delta_5 = 200$ ns with $t_1 = 280$ ns and $t_2 = 480$ ns [see Fig. 7(e)]. The accumulation time of the spectrum, shown in Fig. 7(e), was about 70 h. As can be seen in this case, the absorption line becomes narrower than the usual transmission spectrum obtained without the time-delayed technique [shown in Fig. 7(f)].

Interference of Mössbauer and Rayleigh scattering in the absorber does not play a role in the transmission spectroscopy experiments; see Ref. [20]. This is because the resonant interaction of the radiation field with nuclei takes place due to $M1$ (magnetic dipole) transition, while Rayleigh scattering occurs via electric dipole interaction ($E1$) with atomic electrons. Meanwhile, in reflection geometry, the radiation Bragg scattering in specular fashion (except for the 90° angle of incidence) demonstrates such an interference. For nuclei with

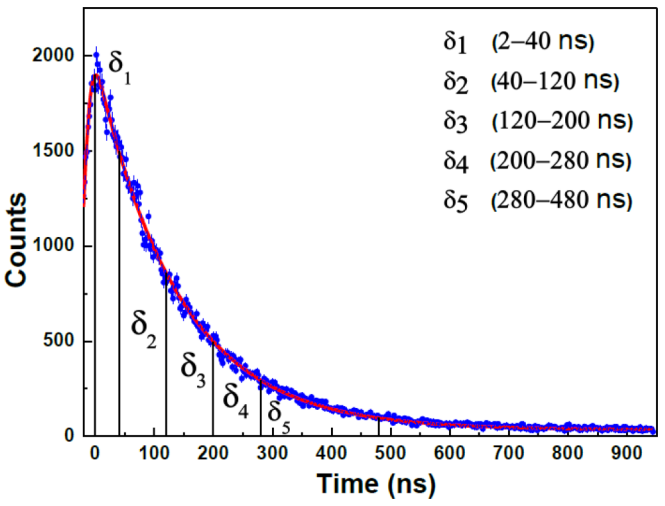

FIG. 6. Decay curve of the radiation field from the source along with time windows $\delta_n(t_1 - t_2)$ where photon counts were collected to plot delayed spectra. The solid red line is a theoretical fitting by an exponent with $T_1 = 141$ ns. Blue dots are experimental data.

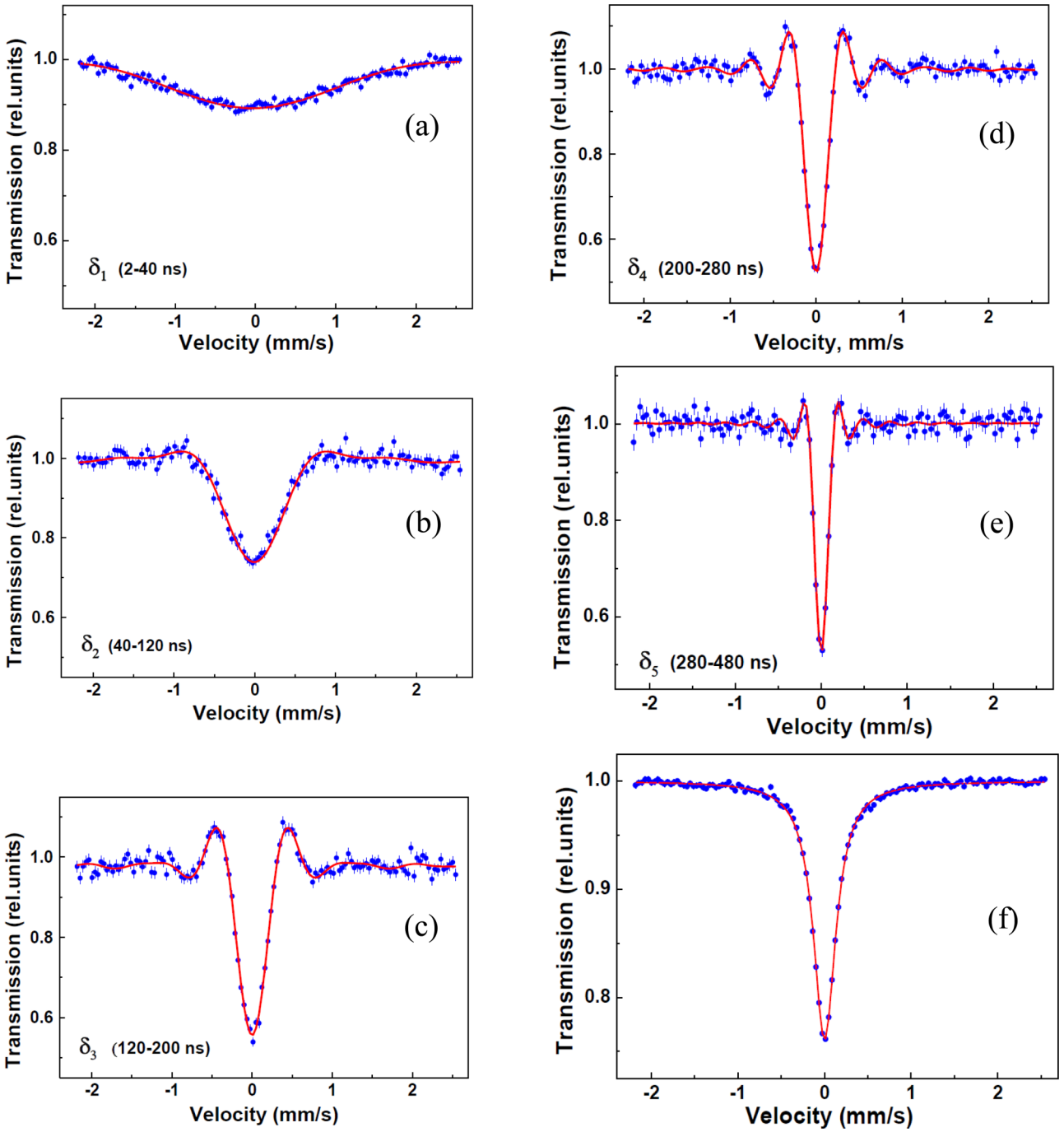

FIG. 7. Transemission spectra obtained with different delay times t_1 and t_2 and different durations of data collection time windows. They are (a) $t_1 = 2$ ns, $t_2 = 40$ ns, and $\delta_1 = 38$ ns; (b) $t_1 = 40$ ns, $t_2 = 120$ ns, and $\delta_2 = 80$ ns; (c) $t_1 = 120$ ns, $t_2 = 200$ ns, and $\delta_3 = 80$ ns; (d) $t_1 = 200$ ns, $t_2 = 280$ ns, and $\delta_4 = 80$ ns; and (e) $t_1 = 280$ ns, $t_2 = 480$ ns, and $\delta_5 = 200$ ns. Conventional spectrum is shown in (f).

a single absorption line, this interference results in asymmetry of experimentally measured spectra [21,22]. Therefore, the symmetry of the spectra, shown in our Fig. 7, and the experimental results obtained by Black and Moon in transmission geometry [20], confirm that the Rayleigh scattering can be disregarded in the transmission experiments as a simple background.

The advantage of using the time-delayed technique is shown here via an example of gamma-resonance measurements with time selection of iron-based nanoparticles on the graphene oxide support. Composite materials comprising metal nanoparticles on a structural support have gained significant attention in recent years as novel systems for a new generation of catalysts, electrode materials in energy conversion and storage devices, and other similar applications. Due to the large surface area, the nanostructured systems possess an apparent advantage over traditional forms of materials. Moreover, iron-containing materials are interesting due to

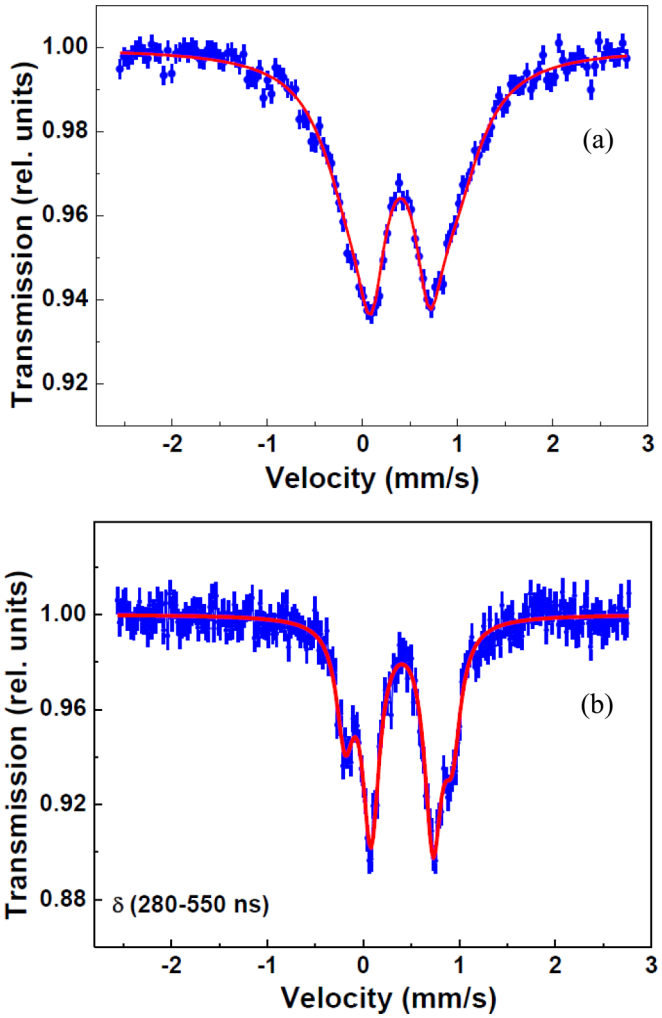

FIG. 8. Transemission spectra of GO containing Fe nanoparticles, which are obtained by conventional Mössbauer spectroscopy (a) and by collecting γ-photon counts in a time window (t_1, t_2), where $t_1 = 280$ ns and $t_2 = 550$ ns (b).

their peculiar electromagnetic and catalytic properties, and the low cost-to-performance ratio.

Graphene oxide (GO) has several apparent advantages as a structural support for growing metal nanoparticles. GO contains oxygen functional groups that facilitate uniform deposition of metals on its surface, and longer exposition, formation, and stabilization of metal clusters. Another advantage of GO is its ability to form stable solutions in several solvents by exfoliating to single-atomic-layer sheets. The solution phase provides easy and unimpeded access of reactants to the GO surface, opening unlimited venues for liquid phase processing. This property of GO makes it possible to uniformly cover the GO surface with nucleation centers of metal nanoclusters made from iron ions present in a bulk salt solution. In our experiment, we have used the solution phase reaction between GO and iron (III) nitrate, $Fe(NO_3)_3$.

The iron ions uniformly cover the GO surface due to the formation of chemical bonding between the Fe(III) cation and GO: the oxygen functional groups of GO serve as ligands, replacing water molecules from the first coordination sphere of the Fe(III) cation. The process can be further complicated by the tendency of Fe(III) to hydrolyze in aqueous solutions. The hydrolysis of Fe(III) ions causes the formation of hydroxocomplexes of iron on the GO surface, i.e., the clusters where several Fe(III) cations bind to each other via the hydroxide ion bridges (OH_-). Undoubtedly, the chemical properties of the material will depend on the presence and number of different types of transition-metal centers present in it.

The Mössbauer spectrum of the as-formed Fe-GO sample is shown in Fig. 8(a). It is a quadrupole doublet with slightly asymmetric lines. The doublet hyperfine parameters are $IS = 0.36$ mm/s, $QS = 0.71$ mm/s, which are the center shift and quadrupole splitting of the lines in the doublet. The line broadening and their amplitude asymmetry can be explained by the distribution of quadrupole splittings and center shifts by the Gol'danskii-Karyagin effect due to texture or by the presence of several centers of iron ions. Unfortunately, mathematical processing of the spectrum cannot give an obvious preference to one of the above explanations. The Mössbauer spectrum of this sample with time selection is shown in Fig. 8(b). The features associated with the presence of two centers of iron atoms are clearly visible in the spectrum. Mathematical treatment of this spectrum actually reveals the presence of two quadrupole doublets with the following hyperfine parameters: $IS = 0.37$ mm/s and $QS = 1.12$ mm/s for one center, and $IS = 0.4$ mm/s and $QS = 65$ mm/s for another center. It is likely that in the as-formed Fe-GO there are two types of iron: the Fe(III) ions bonded to the GO functional groups, and the Fe(III) ions bonded to OH_- with the formation of clusters. Depending on the reaction conditions, the percentage of two types of iron in Fe-GO may vary [23].

V. CONCLUSION

The delayed photon counts technique is promising in optical and gamma-domain Mössbauer spectroscopy. The interference of the incident and coherently scattered radiation fields plays a crucial role in this technique. The radiation field of the source and the radiation field coherently scattered by nuclei in the absorber have different frequencies, i.e., ω_S and ω_A, respectively. Interference of these fields results in intensity beats with a frequency difference $\Delta = \omega_S - \omega_A$. If we do not collect photon counts within a preset time interval $(0, T)$, the phase shift ΔT, accumulated in this interval, will be revealed in the signal detected at a later time. If $T > T_1$, this interference results in the enhancement of spectral resolution.

In spite of a longer time for data collection, this technique can disclose tiny details of the transmission spectra if complete information about the energy-level structure and the number of centers contributing to the observable signals are not known in advance. One can also find another example of the remarkable enhancement of measurement accuracy due to interference phenomena in Refs. [24–27]. Determination of the absorption line position with high accuracy in time-domain experiments employing a modulation technique is described in Refs. [24,25]. This modulation technique also allows us to perform spatial displacement measurements with subangstrom resolution [26,27].

ACKNOWLEDGMENTS

F.G.V. acknowledges partial funding of this work by the Program of Competitive Growth of Kazan Federal University, funded by the Russian Government, and the Russian Foundation for Basic Research (Grant No. 18-02-00845-a).

APPENDIX

For simplicity, we limit our consideration to the case $\Gamma_A = \Gamma_S = \Gamma$. Then, with the help of approximation (33), we calculated analytical expressions for the infinite-time spectrum $n_\infty(\Delta)$, Eq. (20), and spectrum $n_{0T}(\Delta)$, which is detected in a short-time interval, Eq. (23). For the infinite-time spectrum, the result is

$$n_\infty(\Delta) = \frac{1}{\Gamma}\left[1 - (C_1 - C_2)\frac{\Gamma^2}{\Delta^2+\Gamma^2} + 2C_2\frac{\Gamma^4}{(\Delta^2+\Gamma^2)^2}\right], \tag{A1}$$

where $C_1 = a_1 d/2$ and $C_2 = a_2 d^2/8$. Comparison of the approximated result, Eq. (A1), with the exact dependence $n_\infty(\Delta)$, Eq. (20), is shown in Fig. 9(a) for $d = 1$. The approximate dependence fits well with the exact result even for absorbers with moderate thickness.

It is interesting to notice that the spectrum $n_\infty(\Delta)$ consists of two lines. One of the lines, with the coefficient C_1, has a half-width Γ, and the other, with the coefficient C_2, has a half-width $\sqrt{\sqrt{2}-1}\Gamma = 0.644\Gamma$, which is 1.55 times narrower. These lines are subtracted (the narrow from the broad) and the result is the line with increased width.

A half-width Γ_{Th} of this broadened line $n_\infty(\Delta)$ can be calculated from the equation $1 - \Gamma n_\infty(\Gamma_{Th}) = [1 - \Gamma n_\infty(0)]/2$, whose solution is

$$\Gamma_{Th}/\Gamma = \sqrt{\frac{A}{B} + \sqrt{1 + \frac{A^2}{B^2}}}, \tag{A2}$$

where $A = a_2 d/2$ and $B = a_1 - 3a_2 d/4$. For $d \leqslant 1$ this solution can be approximated as

$$\Gamma_{Th}/\Gamma = \sqrt{1 + \tfrac{1}{2}(D + D^2 + D^3 + D^4)}, \tag{A3}$$

where $D = d a_2/a_1$. This equation shows that for the absorber with thickness $T = 1$, the half-width of the transmission line, Γ_{Th}, increases to 1.13Γ, i.e., by 13% compared with the half-width Γ for a very thin sample.

1. Short-time interval $(0, T)$

For a short-time interval $(0, T)$, calculation of the integrals in Eq. (23) with the help of approximation (33) gives

$$n_{0T}(\Delta) = n_\infty(\Delta)(1 - e^{-\Gamma T}) + n_1(\Delta, T) + n_2(\Delta, T), \tag{A4}$$

where

$$n_1(\Delta, T) = \left[C_3\frac{\Gamma \sin \Delta T}{\Delta} - C_4\frac{1 - \cos \Delta T}{\Delta^2} - C_2\Gamma T \cos \Delta T\right] \times \frac{\Gamma e^{-\Gamma T}}{\Delta^2 + \Gamma^2}, \tag{A5}$$

$$C_3 = C_1 - C_2(1 + \Gamma T), \tag{A6}$$

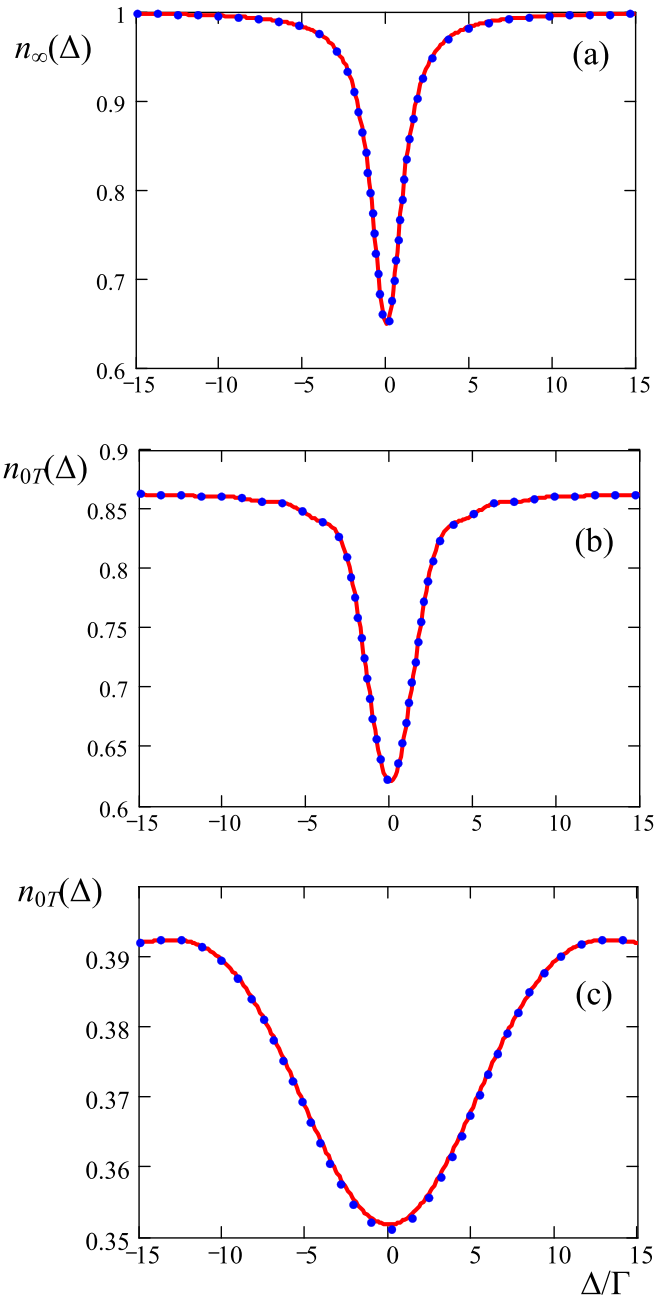

FIG. 9. (a) Dependence of the number of counts on the detuning Δ, which are collected in infinite time windows. The number of counts is normalized to unity for $\Delta = \pm\infty$. The solid red line shows the exact result, Eq. (20), and the dotted blue line demonstrates the approximation Eq. (A1). Spectra $n_{0T}(\Delta)$ for $T = 2T_1$ (b) and $T = T_1/2$ (c), which are calculated with the help of exact equations (21), (28), and (29) (solid red line) and approximation Eq. (A4) (dotted blue line). The optical thickness of the absorber is $d = 1$.

$$C_4 = C_1\Delta^2 + C_2\Gamma^2, \tag{A7}$$

$$n_2(\Delta, T) = 2C_2\left[1 - \cos \Delta T - \left(1 - \frac{\Delta^2}{\Gamma^2}\right)\frac{\Gamma \sin \Delta T}{2\Delta}\right] \times \frac{\Gamma^3 e^{-\Gamma T}}{(\Delta^2 + \Gamma^2)^2}. \tag{A8}$$

Examples of spectra for time intervals $(0, T)$ with different durations of T are shown in Figs. 9(b) and 9(c). When T becomes shorter than the lifetime of the excited state T_1, the spectrum broadens appreciably.

Numerical analysis shows that very thin ($d = 0.2$) and moderately thin ($d = 1$) absorbers have the transmission spectra of almost the same shape and width. However, the values of their dips at resonance are very different. Therefore, to simplify analysis one can consider a very thin absorber with $d \ll 1$ and take into account only the contribution of the terms proportional to C_1, which is linearly dependent on the effective thickness of the absorber, d, and one can disregard the contribution of C_2 proportional to d^2. Then, Eq. (A4) is simplified as follows:

$$n_{0T}(\Delta) = \frac{1}{\Gamma}(1 - e^{-\Gamma T}) - C_1 L_b(\Delta, T), \tag{A9}$$

where

$$L_b(\Delta, T) = \frac{\Gamma}{\Delta^2 + \Gamma^2} - e^{-\Gamma T}\frac{\sin(\Delta T + \psi)}{\Delta\sqrt{1 + \frac{\Delta^2}{\Gamma^2}}}, \tag{A10}$$

$$\psi = \tan^{-1}(\Delta/\Gamma). \tag{A11}$$

Since the shape of the transmission dip is well described by Eq. (A9) for arbitrary absorber thickness, one can substitute the numerical coefficient C_1 in Eq. (A9) by the rescaling parameter

$$K_B(d, T) = \frac{1 - e^{-\Gamma T} - \Gamma n_{0T}(0)}{1 - e^{-\Gamma T}(1 + \Gamma T)}, \tag{A12}$$

and obtain a formula that quantitatively describes the dip in the transmission spectrum (its shape and depth) for an arbitrary value of d. Here, the number of counts $n_{0T}(0)$ for $\Delta = 0$ is calculated numerically with the help of Eq. (21) for a given value of d, which is not small. After such a rescaling, Eq. (A9) describes very well the dip in the transmission spectrum (see Fig. 3) where $d = 4$.

The width of the line $L_b(\Delta, T)$ is defined by the competition of the contributions of two terms in Eq. (A10), i.e., the Lorentzian and sinc function. Numerical analysis shows that if $T = T_1/2$, the transmission line becomes six times broader than the Lorentzian, and if $T = T_1$, the line broadens three times with respect to the line collected in the infinite-time interval $(0, \infty)$.

2. Delayed photon counts

If we collect photon counts in a delayed time interval (T, ∞), the spectrum narrows. This spectrum is described by the simple equation

$$n_{T\infty}(\Delta) = n_\infty(\Delta) - n_{0T}(\Delta). \tag{A13}$$

Now, the broad line $n_{0T}(\Delta)$ is subtracted from the narrow line $n_\infty(\Delta)$, which results in the line narrowing effect. Examples of the line narrowing effect are shown in Fig. 10.

To analyze the line narrowing effect, we express Eq. (A13) as follows:

$$n_{T\infty}(\Delta) = \frac{e^{-\Gamma T}}{\Gamma}\left[1 - \frac{F_1(\Delta, T)\Gamma^2}{\Delta^2 + \Gamma^2} + \frac{F_2(\Delta, T)\Gamma^4}{(\Delta^2 + \Gamma^2)^2}\right], \tag{A14}$$

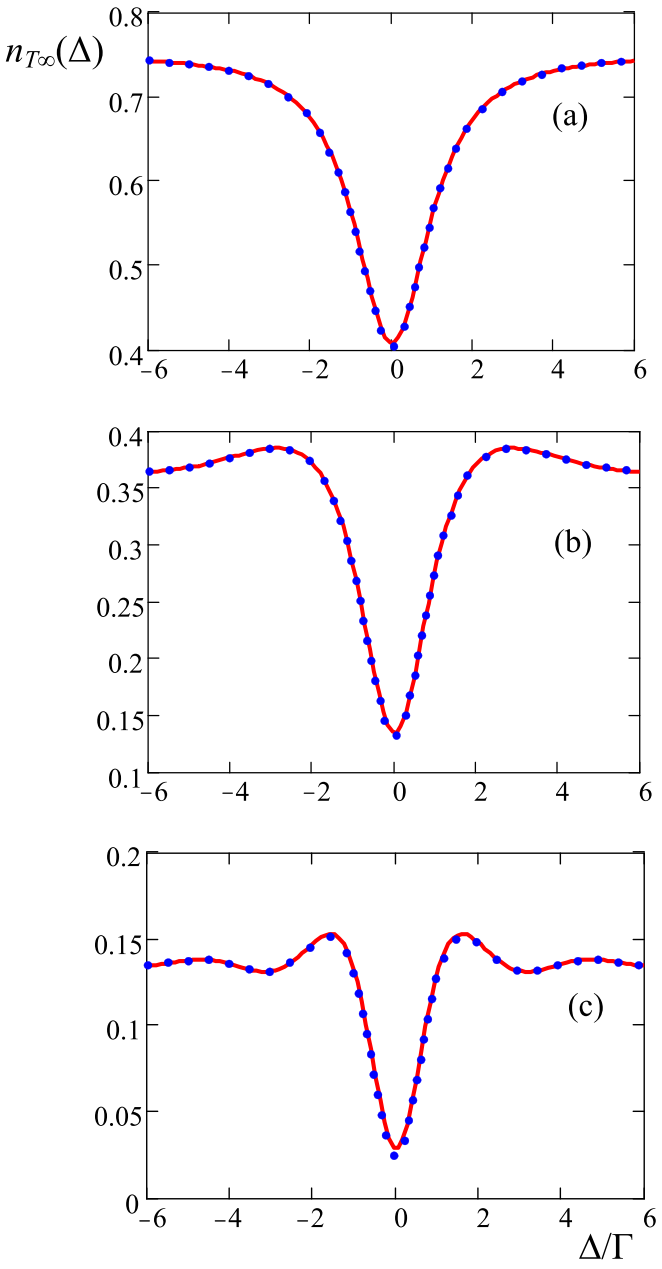

FIG. 10. Time-delayed spectra. Time T when count collection starts is $0.3T_1$ (a), T_1 (b), and $2T_1$ (c). The solid red line corresponds to the exact result. The dotted blue line is plotted with the help of approximation (A14). Optical thickness is $d = 1$.

where

$$F_1(\Delta, T) = C_1 - C_2 + C_3\frac{\Gamma \sin \Delta T}{\Delta} - C_4\frac{1 - \cos \Delta T}{\Delta^2} - C_2\Gamma T \cos \Delta T, \tag{A15}$$

$$F_2(\Delta, T) = 2C_2\left[\cos \Delta T + \left(1 - \frac{\Delta^2}{\Gamma^2}\right)\frac{\Gamma \sin \Delta T}{2\Delta}\right]. \tag{A16}$$

For a thin absorber, the contribution of the term $C_2 = a_2 d^2/8$ could be neglected, and Eq. (A14) is approximated as follows:

$$n_{T\infty}(\Delta) \approx \frac{e^{-\Gamma T}}{\Gamma}\left[1 - C_1\frac{\Gamma^2 \sin(\Delta T + \psi)}{\Delta\sqrt{\Gamma^2 + \Delta^2}}\right]. \tag{A17}$$

Analysis of this expression shows that, for example, for $T = 2T_1 = 2/\Gamma$ the function $\sin(\Delta T + \psi)/\Delta$ reaches its first zero at $\Delta = \pm 1.14\Gamma$. These detunings correspond to the first maxima of the transmission spectra; see Fig. 10. Therefore, the half-width of the absorption dip in the spectrum is located between $\Delta = 0$ and, for example, $\Delta = 1.14\Gamma$. This half-width is equal to 0.57Γ, i.e., it becomes nearly two times smaller than the half-width of the stationary spectrum.

Numerical analysis shows that the negative contribution of the thickness line broadening to the line narrowing effect is quite small in time-delayed photon counts. Following this result, we extend the validity of Eq. (A17) to the case of thick absorbers and rewrite it as follows:

$$n_{T\infty}(\Delta) \approx \frac{e^{-\Gamma T}}{\Gamma}\left[1 - K_{\mathrm{N}}(d,T)\frac{\Gamma^2 \sin(\Delta T + \psi)}{\Delta\sqrt{\Gamma^2 + \Delta^2}}\right], \quad \text{(A18)}$$

where the rescaling coefficient

$$K_{\mathrm{N}}(d,T) = \frac{1 - \Gamma n_{T\infty}(0) e^{\Gamma T}}{1 + \Gamma T} \quad \text{(A19)}$$

is introduced to have a true value of the dip in the transmission spectrum of the absorber with effective thickness $d > 1$. Here $n_{T\infty}(0)$ (not approximated) is calculated with the help of Eqs. (A13), (21), and (32).

[1] C. S. Wu, Y. K. Lee, N. Benczer-Koller, and P. Simms, Phys. Rev. Lett. **5**, 432 (1960).

[2] W. T. Triftshäuser and P. P. Craig, Phys. Rev. Lett. **16**, 1161 (1966).

[3] R. Grim, P. Gütlich, E. Kankeleit, and R. Link, J. Chem. Phys. **67**, 5491 (1977).

[4] P. Novak, J. Pechousek, V. Prochazka, J. Navarik, L. Kouril, P. Kohout, V. Vrba, and L. Machala, Nucl. Instrum. Methods Phys. Res. A **832**, 292 (2016).

[5] D. W. Hamill and G. R. Hoy, Phys. Rev. Lett. **21**, 724 (1968).

[6] W. E. Tefft, Found. Phys. **3**, 255 (1973).

[7] D. P. O'Brien, P. Meystre, and H. Walther, Adv. At. Mol. Phys. **21**, 1 (1985).

[8] I.-J. Ma, J. Mertens, G. zu Putlitz, and G. Schütte, Z. Phys. **208**, 352 (1968).

[9] C. Copley, B. P. Kibble, and G. W. Series, J. Phys. B **1**, 724 (1968).

[10] H. Figger and H. Walter, Z. Phys. **267**, 1 (1974).

[11] H. Metcalf and W. Phillips, Opt. Lett. **5**, 540 (1980).

[12] F. J. Lynch, R. E. Holland, and M. Hamermesh, Phys. Rev. **120**, 513 (1960).

[13] P. Gütlich, E. Bill, and A. X. Trautwein, *Mössbauer Speectroscopy and Transition Metal Chemistry: Fundamentals and Applications* (Springer-Verlag, Berlin, 2011).

[14] E. Varoquaux, G. A. Williams, and O. Avenel, Phys. Rev. B **34**, 7617 (1986).

[15] P. Helistö, I. Tittonen, M. Lippmaa, and T. Katila, Phys. Rev. Lett. **66**, 2037 (1991).

[16] R. N. Shakhmuratov, F. Vagizov, and O. Kocharovskaya, Phys. Rev. A **87**, 013807 (2013).

[17] *Handbook of Mathematical Functions*, edited by M. Abramowitz and I. A. Stegun (Dover, New York, 1965).

[18] A. Vertes, L. Korecz, and K. Burger, *Mössbauer Speectroscopy* (Elsevier, New York, 1979).

[19] R. N. Shakhmuratov, F. Vagizov, and O. Kocharovskaya, Phys. Rev. A **84**, 043820 (2011).

[20] P. J. Black and P. B. Moon, Nature (London) **188**, 481 (1960).

[21] P. J. Black, D. E. Evans, and D. A. O'Connor, Proc. R. Soc. Lond. A **270**, 168 (1962).

[22] P. J. Black, G. Longworth, and D. A. O'Connor, Proc. Phys. Soc. **83**, 925 (1964).

[23] A. Khannanov, A. Kiamov *et al.*, J. Am. Chem. Soc. **140**, 9051 (2018).

[24] J. E. Monahan and G. J. Perlow, Phys. Rev. A **20**, 1499 (1979).

[25] R. N. Shakhmuratov, F. G. Vagizov, M. O. Scully, and O. Kocharovskaya, Phys. Rev. A **94**, 043849 (2016).

[26] R. N. Shakhmuratov and F. G. Vagizov, Phys. Rev. B **95**, 245429 (2017).

[27] R. N. Shakhmuratov and F. G. Vagizov, Pis'ma Zh. Eksp. Teor. Fiz **108**, 785 (2018) [JETP Lett. **108**, 772 (2018)].